OPEN ACCESS
IOP Publishing | Songshan Lake Materials Laboratory
Letters
Materials Futures
Mater. Futures 2 (2023) 021001 (7pp)
https://doi.org/10.1088/2752-5724/acbd64

Letter

Atomically constructing a van der Waals heterostructure of $CrTe_2/Bi_2Te_3$ by molecular beam epitaxy

Jin-Hua Nie, Rui Li, Mao-Peng Miao, Ying-Shuang Fu* and Wenhao Zhang*

School of Physics and Wuhan National High Magnetic Field Center, Huazhong University of Science and Technology, Wuhan 430074, People's Republic of China

E-mail: wenhaozhang@hust.edu.cn and yfu@hust.edu.cn

Received 16 December 2022, revised 16 February 2023
Accepted for publication 19 February 2023
Published 15 March 2023

Abstract

A 2D heterostructure with proximity coupling of magnetism and topology can provide enthralling prospects for hosting new quantum states and exotic properties that are relevant to next-generation spintronic devices. Here, we synthesize a delicate van der Waals (vdW) heterostructure of $CrTe_2/Bi_2Te_3$ at the atomic scale via molecular beam epitaxy. Low-temperature scanning tunneling microscopy/spectroscopy measurements are utilized to characterize the geometric and electronic properties of the $CrTe_2/Bi_2Te_3$ heterostructure with a compressed vdW gap. Detailed structural analysis reveals complex interfacial structures with diversiform step heights and intriguing moiré patterns. The formation of the interface is ascribed to the embedded characteristics of $CrTe_2$ and Bi_2Te_3 by sharing Te atomic layer upon interfacing, showing intercoupled features of electronic structure for $CrTe_2$ and Bi_2Te_3. Our study demonstrates a possible approach to construct artificial heterostructures with different types of ordered states, which may be of use for achieving tunable interfacial Dzyaloshinsky–Moriya interactions and tailoring the functional building blocks in low dimensions.

Keywords: molecular beam epitaxy, scanning tunneling microscopy/spectroscopy, 2D heterostructure, interfacial structures

1. Introduction

The explosive growth of 2D materials has given rise to a rich variety of long-range ordered quantum states that have been unprecedentedly uncovered in reduced dimensions, such as low-dimensional superconductivity [1, 2], ferroelectricity [3], ferromagnetism [4, 5] and antiferromagnetism [6]. The weak van der Waals (vdW) coupling further inspires intensive studies with an additional degree of freedom to artificially twist/stack/intercalate each 2D piece, giving rise to a series of exotic quantum phenomena, including chiral Majorana fermions [7], unconventional superconductivity [8], quantum anomalous Hall effect [9] and magnetic skyrmions [10]. In this light, 2D heterostructure of various ingredients can be greatly functionalized with modulated electronic properties while simultaneously possessing nontrivial topology, magnetism and correlated interaction. These strategies have been implemented in many heterostructures. For instance, unusual electronic states and the

* Authors to whom any correspondence should be addressed.

Future perspectives
Constructing heterostructure is a powerful strategy to comprehensively utilize functionalized properties of individual constituents in 2D materials by selective and controllable manipulation of nontrivial topology, magnetism and correlated interaction. Recent advances have achieved many unprecedented quantum phenomena in superlattice and heterostructures, including unconventional superconductivity, quantum anomalous Hall effect, chiral Majorana fermions and magnetic skyrmions. Delicate molecular beam epitaxy offers a promising route to synthesize self-assembly and artificial structures with precise fabrication at atomic scale. Combined with the high-resolution real-space structural/electronic characterization at atomic level by scanning tunneling microscopy/spectroscopy (STM/STS), new ways will be visioned to explore the buried interface with hybridized interaction in the heterostructure. These unique advantages will facilitate the realization of proximity coupling, as well as the achievement of precise detection and tunability, in low-dimensional physics and quantum materials

superconducting proximity effect of Bi(110) films can be modulated by $NbSe_2$ [11], and topological superconductivity with 1D Majorana edge modes was reported when the ferromagnetic $CrBr_3$ is coupled with a superconducting $NbSe_2$ substrate [12], quantum anomalous Hall effect can be realized in proximity-coupled (Zn,Cr)Te/$(Bi,Sb)_2Te_3$/(Zn,Cr)Te [13] and Cr:Sb_2Te_3/Cr_2O_3 [14] heterostructures, as well as in twisted bilayer graphene aligned to hexagonal boron nitride [15], heavy fermions can artificially emerge in a 1T/1H-TaS_2 heterostructure by the Kondo coupling between localized magnetic moments and itinerant electrons [16], etc. Thus, artificial heterostructures offer a fantastic avenue to engineer 2D materials as building blocks with desired properties.

Seeking magnetic skyrmions, local swirls with topologically nontrivial chiral spin textures, is a typical example of taking full advantage of the hybrid systems [17]. To generate and stabilize the noncollinear Dzyaloshinskii–Moriya interaction (DMI), a decisive factor to realize skyrmions that combines the strong spin–orbit coupling (SOC) with broken inversion symmetry at an interface [18], various kinds of artificial heterostructures are theoretically proposed and experimentally fabricated, including ferromagnet/heavy-metal [19], ferromagnet/topological insulator [20], topological insulator/magnetic insulator [21] and heavy-metal/magnetic insulator [22]. To possess the essential characteristic of large SOC, the prototypical topological insulator Bi_2Te_3 with nontrivial surface states is commonly selected to mediate DMI. In addition, Cr_xTe_y compounds, a newly discovered family of 2D vdW magnets that manifest fruitful structural phases and magnetic properties at stable states [23–25] have recently been widely considered to favor strong interfacial DMI and the formation of skyrmions. Néel-type skyrmion lattice was predicted in the $CrTe_2$/WTe_2 bilayer [26], and giant interfacial topological Hall effect was achieved to confirm the topological spin texture of skyrmions in both $CrTe_2$/Bi_2Te_3 and Cr_2Te_3/Bi_2Te_3 hybrid systems [27, 28]. Strikingly, it was argued that the existence of Bi bilayer nanosheets intercalated at the interface of $CrTe_2$ and Bi_2Te_3 should be indispensable to the formation of magnetic skyrmions [28–30]. Such a prerequisite for the interface is subtly coincident with another skyrmion heterostructure of $Mn(Bi,Sb)_2Te_4$ sandwiched by $(Bi,Sb)_2Te_3$, where the thickness of the $(Bi,Sb)_2Te_3$ spacer layer is essential to control the coupling between the gapped topological surface states in the two $Mn(Bi,Sb)_2Te_4$ layers to stabilize the skyrmion formation [31]. This crucially calls for a thorough understanding of the interfacial structure in topological insulator/magnet heterostructure.

In this study, we demonstrate the achievement of vdW epitaxial growth for a high-quality $CrTe_2$/Bi_2Te_3 heterostructure by molecular beam epitaxy (MBE). The $CrTe_2$/Bi_2Te_3 heterostructure processes all the essential ingredients for the formation of magnetic skyrmions: (i) inversion symmetry breaking, (ii) large SOC, and (iii) the entanglement of magnetism and strong SOC. Moreover, the superiority of heterostructures also lies in the advantages of the fabrication aspect. $CrTe_2$ and Bi_2Te_3 are both simple telluride compounds sharing similar hexagonal surface lattice symmetry and the vdW interlayer coupling will facilitate reduced dimension with controlled thickness, the atomically sharp interface and flexibility in stacking order. These all favor the generation of strong interfacial DMI and topological spin textures in real space. In a step-by-step way, the atomic morphologies with sharp interface structure are demonstrated by low-temperature STM/STS measurements. Intriguingly, compared to the bulk $CrTe_2$, our $CrTe_2$ layer shows a $\sim$28% compressed vdW gap with respect to the underlying Bi_2Te_3, which is only half that of the single-monolayer (ML) $CrTe_2$/graphene films. Specifically, we observe a 3.5 nm moiré superstructure with a step height of 0.44 nm, but a 0.40 nm step on the same $CrTe_2$ terrace without moiré patterns. Meanwhile, the real-space STS distribution shows a smooth evolution when crossing the step boundaries from the Bi_2Te_3 to the $CrTe_2$ segments, exhibiting evident interfacial states at the step boundaries. Based on the high Te chemical potential growth conditions and shared Te atomic layers, we propose a schematically structural model of $CrTe_2$ pieces embedded in Bi_2Te_3 films, reasonably reproducing the observed 40 pm difference in height, as well as the emergence of moiré periodicity. Our work not only shields light from constructing 2D heterostructures with different functionalities between topology and magnetism that are interlayer coupled, but also provides a versatile material platform for exploring magnetic skyrmions with tunable DMI and topological properties at the interface.

2. Methods

The $CrTe_2$/Bi_2Te_3 heterostructure was fabricated through a standard MBE growth process in an ultrahigh vacuum chamber at a base pressure of 5×10^{-10} Torr. Prior to growth, a uniform bilayer graphene substrate was obtained as previously reported [32]. The SiC substrate was first degassed at 600 °C for 3 h, then annealed at 950 °C under a Si flux for

ten cycles, and further flashed to 1400 °C for 10 min. The high purity of Bi (99.999%) and Te (99.999%) sources was co-evaporated from two homemade thermal effusions with a large Te:Bi flux ratio of ∼15. The graphene-covered SiC substrate was held at 260 °C during the growth, which was monitored with an infrared spectrometer with an emissivity of 0.9. After growth, the Bi_2Te_3 films were post annealed at the growth temperature for 5 min with a Te flux to improve the crystalline quality, which was also checked by STM measurements before capping the $CrTe_2$ layers. The $CrTe_2$ films were further grown onto the Bi_2Te_3 films by co-evaporating high-purity Cr (99.995%) and Te (99.999%) atoms with a Te:Cr flux ratio of ∼20 while the substrate was kept at 300 °C.

Low-temperature STM/STS measurements were performed on a Unisoku 1500 STM system operating at 4.5 K, if not specifically noted [33]. The normal W tip by electrochemical etching was cleaned by e-beam heating to ∼1800 °C to remove oxides. Prior to STM measurements, the W tip was calibrated on Ag(111)/Si islands. All topographic images were taken in a constant-current mode, and the tunneling dI/dV spectra and conductance mappings were acquired using a standard lock-in technique at 983 Hz with a modulation voltage amplitude of 1% of the set bias voltage. The topographic images were processed using software from WSxM and Gwyddion.

3. Results

Figure 1(a) is an atomic structural model of $CrTe_2/Bi_2Te_3$ heterostructure from a side view. Bi_2Te_3 crystallizes in a tetradymite-type structure with the space group viewed in a layered structure. It stacks in a sequence of Te-Bi-Te-Bi-Te atomic layers along the crystallographic c direction, forming a quintuple layer (QL) with a height of 1 nm. As a result, there are two inequivalent Te and Bi lattice sites, respectively [34]. On the other hand, $CrTe_2$ is in a trigonal layered structure with the space group of $R\bar{3}m1$. Each Cr cation is centered by a Te octahedron with a 1 T structure, analogous to other TMDs [35]. Although bulk $CrTe_2$ crystals and thin films of 1–20 ML had already been identified in a ferromagnetic ground state with a Curie temperature above room temperature [36–38], its single-layer film grown on graphene substrate demonstrated an intriguing antiferromagnetic order and field-induced spin reorientation by real-space observation of spin-polarized STM measurements [39]. The mutability of magnetism in $CrTe_2$ films indicates that some external perturbations of charge transfer, strain, film thickness and interlayer coupling may bring about new issues regarding the heterostructure [40]. Here, due to the inert graphene substrate and weak vdW bonds of both Bi_2Te_3 and $CrTe_2$ layers, the stacking combinations and film thicknesses of $CrTe_2/Bi_2Te_3$ heterostructure can be well controlled by adjusting the MBE growth conditions.

Figure 1(b) is a typical STM image of a bare Bi_2Te_3 film with a nominal thickness of ∼2.6 QL. The surface is atomically flat and smooth, with terraces as large as ∼100 nm, which terminate in a triangular Te-1 × 1 lattice with an in-plane lattice constant of 0.44 nm, as shown in figure 1(c). All edges of the Bi_2Te_3 islands can be well determined as 120°-orientated, conforming to their three-fold crystal symmetry. We record the evolution of dI/dV spectra near the Fermi level (E_F) by STS measurements for various thicknesses of Bi_2Te_3 films in figure 1(d), which is proportional to the local density of states (LDOS). It is apparent that the STS spectrum exhibits a rather flat minimum around 300 meV below E_F for 1 and 2 QL, indicating the intrinsic bulk band insulator of Bi_2Te_3 [7]. As the thickness increases up to 3 QL, a 'V'-shaped LDOS minimum is formed near −140 meV, within the energy range between the bulk valence band maximum and conduction band minimum, suggesting the appearance of the topological surface state by the Dirac-cone band structure. The Dirac point shifts upwards −120 meV for the 4 QL, associated with the apparent quantum well states in both valence and conduction bands as well. This topological transition of the surface states in Bi_2Te_3 ultrathin films at 3 QL is well consistent with previous studies [7, 41]. Here, E_F lies inside the bulk gap for all thicknesses, indicating that the surface carrier density dominates rather than the bulk contribution.

After depositing $CrTe_2$ layers, the morphology shown in figure 1(e) still remains atomically continuous with little changed surface roughness, implying that the interface of the heterostructure should be atomically sharp. Figure 1(f) presents the atomic resolution STM image of the $CrTe_2$ surface, displaying a triangular lattice with an in-plane constant of 0.39 nm. Moreover, two 60° rotated domains exist, within which a clear 2 × 1 superstructure is obviously observed. As elucidated in our previous work in [39], this 2 × 1 periodicity is closely related to its antiferromagnetic spin texture, and can be regarded as a hallmark of the formation of $CrTe_2$ films. This rules out the possibility of $CrTe_3$ and other Cr_xTe_y compounds in our samples [42], also confirming the high crystalline quality of the grown heterostructure. Since the exposed Bi_2Te_3 and capped $CrTe_2$ surfaces can coexist, which is verified by the atomic resolution, we compare the tunneling spectrum of the underneath Bi_2Te_3 and topmost $CrTe_2$ layers in figure 1(g). We find that Bi_2Te_3 exhibits similar DOS before and after the deposition of $CrTe_2$ films. The Dirac point further shifts to −80 meV, approaching E_F, indicating that the $CrTe_2$ layer effectively serves as a p-doping source to Bi_2Te_3 [43]. This can be attributed to the consumption of Te layers in Bi_2Te_3 during the growth of $CrTe_2$, which will be discussed later. In addition, the STS spectrum of the $CrTe_2$ surface on a large energy scale also bears a striking resemblance to the $CrTe_2$/graphene samples [39, 42], suggesting the flexibility of retaining the properties of separate segments in $CrTe_2/Bi_2Te_3$ heterostructure by vdW epitaxial synthesis.

Zooming into the $CrTe_2$ surface, pronounced periodic patterns can be clearly resolved, associated with atomically sharp boundaries that separate $CrTe_2$ and Bi_2Te_3, as displayed in figures 1(e) and 2(a). From the atomically resolved STM image, the moiré periodicity is measured as 3.50 ± 0.02 nm, which suitably matches nine times that of the $CrTe_2$ lattice

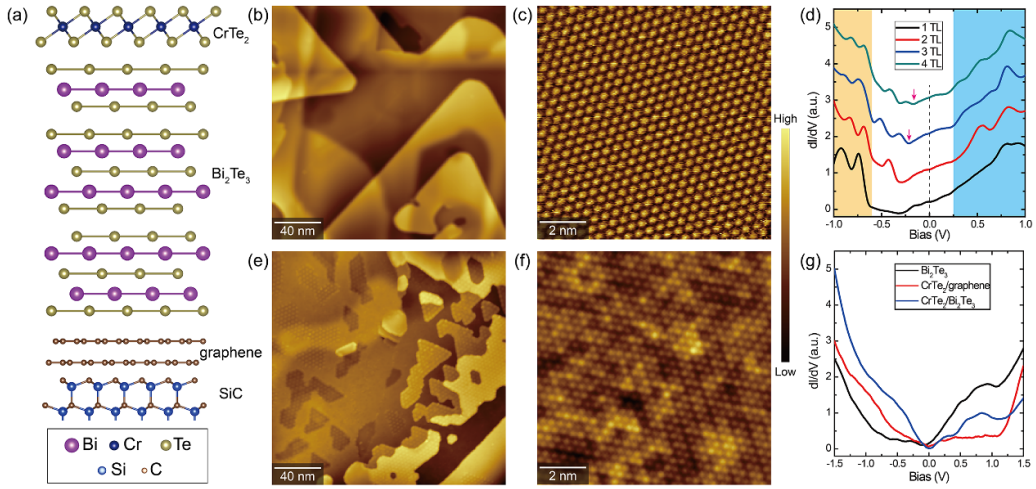

Figure 1. Crystallinity and morphology of the $CrTe_2/Bi_2Te_3$ heterostructure. (a) Side view of atomic structural model of a $CrTe_2/Bi_2Te_3$ heterostructure grown on a bilayer graphene-covered SiC substrate. Thicknesses of $CrTe_2$ and Bi_2Te_3 layers are selected as 1 ML and 2.5 QL, respectively. Both sides of all vdW gaps between $CrTe_2$-$CrTe_2$, Bi_2Te_3-Bi_2Te_3 and $CrTe_2$-Bi_2Te_3 are occupied by Te atoms. (b) Large-scale STM morphology of pristine Bi_2Te_3 films (200×200 nm^2, $V_{bias} = +3.0$ V, $I_t = 10$ pA). (c) Atomically resolved STM image for the Bi_2Te_3 surface in (b) (10×10 nm^2, $V_{bias} = +0.1$ V, $I_t = 100$ pA). (d) Typical tunneling spectra of the Bi_2Te_3 films with various thicknesses. Dashed vertical line is the Fermi energy, and the shaded cyan region indicates the energy of conduction bands. Set point: $V_{bias} = +1.0$ V, $I_t = 100$ pA, and $V_{mod} = 10$ mV. (e) STM morphology of $CrTe_2$ surface grown on Bi_2Te_3 films of (b) (200×200 nm^2, $V_{bias} = +3.0$ V, $I_t = 10$ pA). (f) Atomically resolved STM image for the $CrTe_2$ surface in (e) (10×10 nm^2, $V_{bias} = +0.1$ V, $I_t = 100$ pA). (g) STS spectra for the Bi_2Te_3 and $CrTe_2$ surface, respectively. dI/dV on $CrTe_2$/graphene is also shown for comparison. Set point: $V_{bias} = +1.5$ V, $I_t = 100$ pA, and $V_{mod} = 15$ mV.

constant ($0.389 \times 9 = 3.501$ nm) and eight times that of Bi_2Te_3 ($0.438 \times 8 = 3.504$ nm). This is well in accordance with our simulated pattern of 3.5 nm periodicity by overlaying atomic structures of Bi_2Te_3 and $CrTe_2$, as compared in figure 2(b). This agreement also validates that the terminated Te atoms of both Bi_2Te_3 and $CrTe_2$ should be aligned along the same direction without any twisted angle [10]. In addition to the morphologies, the 3.5 nm moiré pattern can also be reflected by the electronic structure. In figure 2(e), we plot the spatial STS distributions along the moiré structure, and examine the conductance spectra at different sites with atomic precision. Explicitly, an electronic modulation of 3.5 nm is resolved, agreeing well with the moiré periodicity. This demonstrates the ability to tune the local electronic structure as a function of atomic registry in $CrTe_2/Bi_2Te_3$ heterostructure.

Surprisingly, we find that the apparent step height of $CrTe_2$ films is about 0.44 ± 0.05 nm, which is largely reduced compared to the $CrTe_2$/graphene films or the bulk value of 0.62 nm. The height is also strongly sensitive to different applied biases, as shown in figures 2(c) and (d). Generally, there are three aspects in the atomic height of $CrTe_2/Bi_2Te_3$ that are different to 1 ML $CrTe_2$/graphene, which ranges from 0.88–1.05 nm [39]. (i) The former manifests an averaged 29% reduction compared to the bulk, while the latter is 58% larger than the bulk value. (ii) The evolution of the apparent height in 1 ML $CrTe_2/Bi_2Te_3$ can be roughly classified as a slightly larger value for the fulfilled states and a smaller height for the unoccupied ones, with little change for the negative (positive) biases. However, the height of 1 ML $CrTe_2$/graphene shows a monotone decline with increasing bias voltages. (iii) We also observe a global 0.04 nm lower terrace than the 0.44 nm $CrTe_2$ above Bi_2Te_3, accompanied by the disappearance of moiré patterns, as compared in figures 2(a) and (c). To check the difference between the regions with and without moiré patterns, we acquire STM images on the same $CrTe_2$ surface across their boundaries at different biases in figures 2(f) and (g). The atomically resolved topographies clearly verify that the Te atoms are uninterrupted in a perfect triangular lattice around the borders, while the 0.04 nm corrugation remains.

To gain more insight into the $CrTe_2$-Bi_2Te_3 interface, we perform detailed spatially dependent dI/dV measurements across the step boundaries between the Bi_2Te_3 and $CrTe_2$ terraces. As shown in figures 3(a) and (b), the STS around the boundry exhibits strong spectrum shifts that are distinct from both Bi_2Te_3 and $CrTe_2$, an indicator for the formation of interfacial states. Interestingly, Bi_2Te_3 and $CrTe_2$ all show an overall V-shaped landscape with a conductance minimum near E_F, which is different to the isolated Bi_2Te_3 and $CrTe_2$ cases in figure 1(g). Simultaneously, the STS line cut shows a smooth transition from Bi_2Te_3 and $CrTe_2$, with the crossover region distributed around the step boundaries. The similarity of STS between Bi_2Te_3 and $CrTe_2$ suggests that they should be intercoupled with each other and electronically hybridized at the interface, which conversely modifies the structural morphologies of the $CrTe_2$-Bi_2Te_3 interface with changing step height. The common Te-terminated surface, clean structure and transitional electronic properties at the interface suggest that the topological surface states of Bi_2Te_3 are permitted to extend

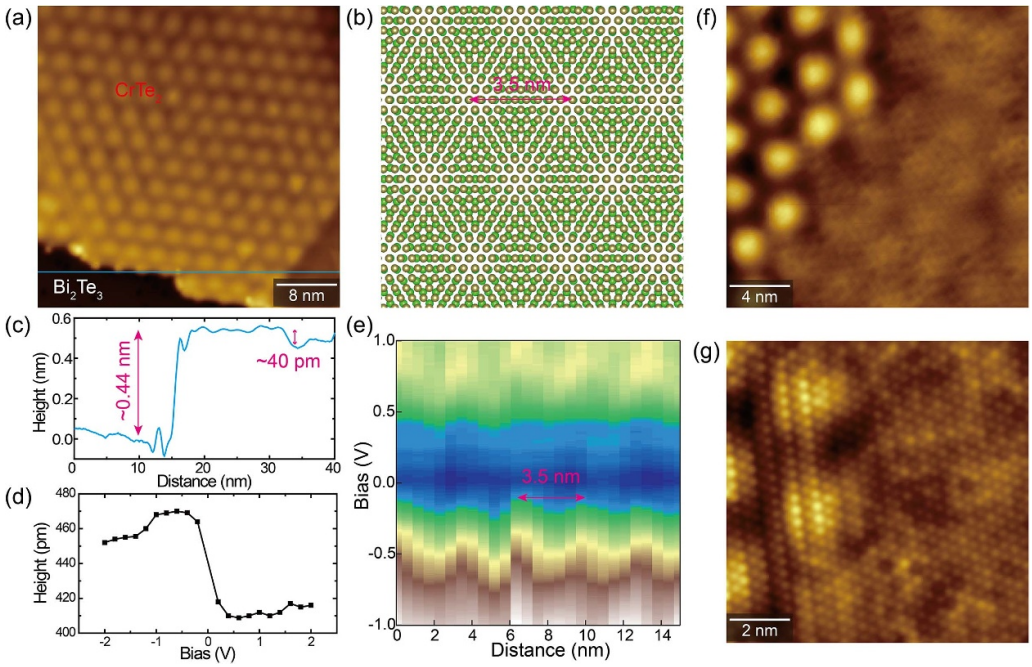

Figure 2. Moiré structure of the $CrTe_2/Bi_2Te_3$ heterostructure. (a) STM morphology of a 1 ML $CrTe_2$ layer supported by a 4 QL Bi_2Te_3 film (40×40 nm^2, $V_{bias} = +1.0$ V, $I_t = 50$ pA). (b) Simulated pattern of two pieces of $CrTe_2$ and Bi_2Te_3 layers when they are aligned in the same direction, reproducing the 3.5 nm moiré patterns in (a). (c) Line profile taken along the cyan line in (a). (d) Apparent height of 1 ML $CrTe_2$ terrace grown on Bi_2Te_3 films at different tunneling biases. (e) 2D plot of tunneling spectra measured along the moiré structure in (a) (Set point: $V_{bias} = +1.0$ V, $I_t = 100$ pA, and $V_{mod} = 10$ mV). A 3.5 nm electronic modulation is clearly resolved, consistent with the moiré periodicity in STM morphology. (f) STM image containing the 1 ML $CrTe_2$ layer with and without moiré patterns, distinguished by the bright (dark) contrast (20×20 nm^2, $V_{bias} = +0.8$ V, $I_t = 100$ pA). (g) Similar region of (g) but taken at a smaller bias voltage. While the contrast remains, Te atoms are found to be continuous across the boundaries (10×10 nm^2, $V_{bias} = +0.03$ V, $I_t = 150$ pA).

into the magnetic $CrTe_2$ layers, facilitating efficient magnetic exchange coupling and the hybridization of Bi p-orbitals and Cr d-orbitals to greatly enhance the DMI. Recent theoretical simulations on a similar $CrTe_2/Bi_2Te_3$ [27] and Cr_2Te_3/Bi_2Te_3 [28] heterostructure have demonstrated the formation of Néel-textured magnetic skyrmions at the interface. Moreover, the enhanced DMI strength is calculated to be 36 pJ m^{-1} for a 6 nm $CrTe_2$ layer, and the skyrmion size in $CrTe_2/Bi_2Te_3$ heterostructure is estimated to be a maximum value of 34 nm [27].

Although there have been several reports on the growth of Cr_xTe_y/Bi_2Te_3 heterostructure by the MBE method [27, 28, 30], the compositive phase and detailed interface structure may be diverse from each other, where the growth temperature is argued to play a key role in forming the specific heterostructure. Generally, lower substrate temperature is favorable for forming Cr_2Te_3 phase, while a higher substrate temperature is more propitious to obtaining $CrTe_2$ phase. This is well consistent with our previous study, which found that $CrTe_3$ can be gradually transformed into $CrTe_2$ by further *in situ* vacuum annealing [42]. On the other hand, due to the high volatility of Te atoms at elevated temperature, the effective flux of the Te source should be decreased and become insufficient to sustain the Te-rich environment. Moreover, Cr atoms have stronger reducibility than Bi atoms, making it possible for Cr atoms to extract Te atoms from Bi_2Te_3 layer once the Te is in short supply, or Cr can even replace Bi atoms, thus forming a new Cr_2Te_3 layer. Considering the three- and five-atomic-layered structure of $CrTe_2$ and Bi_2Te_3, respectively, both sharing the common Te layers on both sides of the vdW gap, we thus construct a possible structural model by stacking a 5 ML $CrTe_2$ embedded in a 3 QL Bi_2Te_3 film, as illustrated in figure 3(c). We speculate that, during the growth, the prophase of existing Te layers of Bi_2Te_3 can also serve as a Te source to help form the adhered $CrTe_2$ layers. This means that the adjacent $CrTe_2$ and Bi_2Te_3 will share the same Te atoms, especially when their Te atoms are very close, as marked by red dashed circles. Accordingly, the Bi_2Te_3 film becomes deficient in Te atoms and more p-doped [43], consistent with the shift of the Dirac point in figure 3(b). In addition, the locations of vdW gaps in $CrTe_2$ and Bi_2Te_3 become mismatched laterally, and the step height significantly deviates from the bulk value. In figure 3(c), the embedded structure can produce both 0.44 and 0.40 nm atomic heights between the $CrTe_2$ and Bi_2Te_3 terraces, reasonably agreeing with our STM observations in figure 2. Moreover, the variation of moiré patterns on the same $CrTe_2$ terrace with a slight height difference can now be well understood. When the heterostructure interface is formed between both Te layers of $CrTe_2$ and Bi_2Te_3, the step is 40 pm higher with moiré periodicity. Otherwise, this moiré superstructure would be invisible when the Te layer of

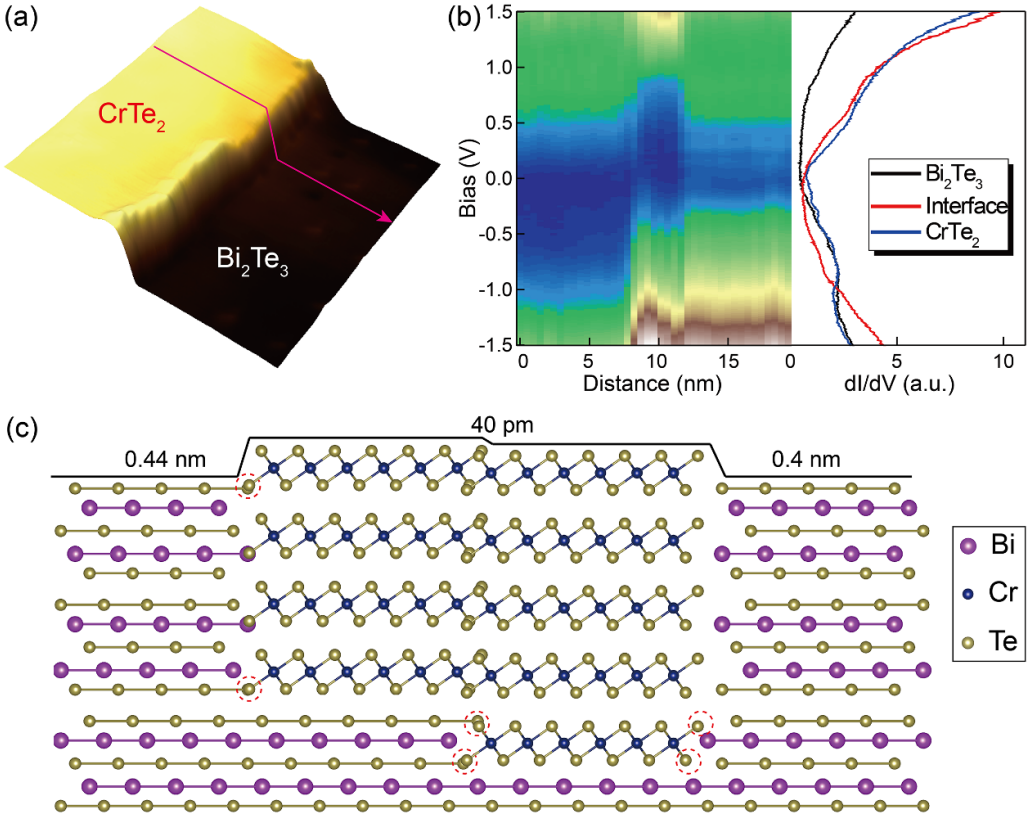

Figure 3. Atomic and electronic structure of the $CrTe_2/Bi_2Te_3$ interface. (a) STM image of a sharp step between $CrTe_2$ and Bi_2Te_3 films (20×20 nm^2, $V_{bias} = +1.5$ V, $I_t = 50$ pA). (b) Left panel: a series of 2D plots of tunneling spectra measured along the arrow in (a). Right panel: Selected dI/dV spectra for $CrTe_2$, $CrTe_2$-Bi_2Te_3 interface and Bi_2Te_3 films, respectively (Set point: $V_{bias} = +1.5$ V, $I_t = 100$ pA, and $V_{mod} = 15$ mV). (c) Possible atomic structure of the $CrTe_2/Bi_2Te_3$ interface. Close-by Te atoms, which belong to the $CrTe_2$ and Bi_2Te_3 layers, respectively, are marked by red dashed circles.

$CrTe_2$ interacts with the Bi layer of Bi_2Te_3. In this light, our structural and electronic observations of the $CrTe_2/Bi_2Te_3$ heterostructure directly reflect a much more contractive vdW gap at the interface, with distinct electronic properties from the $CrTe_2$/graphene case, where the vdW gap is largely expended [39]. It is worth noting that other possibilities may exist, except for the above five layers of $CrTe_2$, whereas the commonly observed compressed steps of overlaid $CrTe_2$ layers imply that there may be many other combinations of sharing Te layers between $CrTe_2$ and Bi_2Te_3, in accordance with our embedded scenario.

4. Conclusion

We study the vdW epitaxial growth of two 2D materials, $CrTe_2$ and Bi_2Te_3, using the MBE technique. We unravel the detailed morphological and electronic structures of the $CrTe_2/Bi_2Te_3$ heterostructure with the emergence of moiré patterns, which are strongly dependent on the step height of the $CrTe_2$ layer. The STS also shows a spectroscopic similarity between $CrTe_2$ and Bi_2Te_3 with a crossover in the interfacial region. We provide an embedded structural model with a shared Te atomic layer at the interface to form a mismatched and compressed interface in the $CrTe_2/Bi_2Te_3$ heterostructure. Our results manifest a promising route to tailor unprecedented quantum states with versatile tunability by interface engineering in 2D vdW heterostructures.

Acknowledgments

This work is funded by the National Key Research and Development Program of China (Grant Nos. 2022YFA1402400, 2018YFA0307000 and 2019YFA0308603) and the National Natural Science Foundation of China (Grant Nos. 12174131, 92265201, 11774105, 11874161, 11934020, 12174443 and U20A6002).

ORCID iDs

Ying-Shuang Fu https://orcid.org/0000-0001-7876-2812
Wenhao Zhang https://orcid.org/0000-0003-2386-0305

References

[1] Sacépé B, Feigelman M and Klapwijket T M 2020 Quantum breakdown of superconductivity in low-dimensional materials *Nat. Phys.* **16** 734–46
[2] Devarakonda A, Inoue H, Fang S, Ozsoy-Keskinbora C, Suzuki T, Kriener M, Fu L, Kaxiras E, Bell D C and Checkelsky J G 2020 Clean 2D superconductivity in a bulk van der Waals superlattice *Science* **370** 231–6

[3] Chang K *et al* 2016 Discovery of robust in-plane ferroelectricity in atomic-thick SnTe *Science* **353** 274
[4] Burch K S, Mandrus D and Park J-G 2018 Magnetism in two-dimensional van der Waals materials *Nature* **563** 47–52
[5] Gong C and Zhang X 2019 Two-dimensional magnetic crystals and emergent heterostructure devices *Science* **363** 706
[6] Valenzuela S O and Roche S 2019 The phase diagram of 2D antiferromagnets *Nat. Nanotechnol.* **14** 1088–9
[7] Xu J-P *et al* 2015 Experimental detection of a Majorana mode in the core of a magnetic vortex inside a topological insulator-superconductor $Bi_2Te_3/NbSe_2$ heterostructure *Phys. Rev. Lett.* **114** 017001
[8] Cao Y, Fatemi V, Fang S, Watanabe K, Taniguchi T, Kaxiras E and Jarillo-Herrero P 2018 Unconventional superconductivity in magic-angle graphene superlattices *Nature* **556** 43–50
[9] Chang C-Z *et al* 2013 Experimental observation of the quantum anomalous Hall effect in a magnetic topological insulator *Science* **340** 167
[10] Heinze S, von Bergmann K, Menzel M, Brede J, Kubetzka A, Wiesendanger R, Bihlmayer G and Blügel S 2011 Spontaneous atomic-scale magnetic skyrmion lattice in two dimensions *Nat. Phys.* **7** 713–8
[11] Peng L, Qiao J, Xian J-J, Pan Y, Ji W, Zhang W and Fu Y-S 2019 Unusual electronic states and superconducting proximity effect of Bi films modulated by a $NbSe_2$ substrate *ACS Nano* **13** 1885–92
[12] Kezilebieke S, Huda M N, Vaňo V, Aapro M, Ganguli S C, Silveira O J, Głodzik S, Foster A S, Ojanen T and Liljeroth P 2020 Topological superconductivity in a van der Waals heterostructure *Nature* **588** 424
[13] Watanabe R, Yoshimi R, Kawamura M, Mogi M, Tsukazaki A, Yu X Z, Nakajima K, Takahashi K S, Kawasaki M and Tokura Y 2019 Quantum anomalous Hall effect driven by magnetic proximity coupling in all-telluride based heterostructure *Appl. Phys. Lett.* **115** 102403
[14] Pan L *et al* 2020 Observation of quantum anomalous Hall effect and exchange interaction in topological insulator/antiferromagnet heterostructure *Adv. Mater.* **32** 2001460
[15] Serlin M, Tschirhart C L, Polshyn H, Zhang Y, Zhu J, Watanabe K, Taniguchi T, Balents L and Young A F 2020 Intrinsic quantized anomalous Hall effect in a moiré heterostructure *Science* **367** 900
[16] Vaňo V, Amini M, Ganguli S C, Chen G, Lado J L, Kezilebieke S and Liljeroth P 2021 Artificial heavy fermions in a van der Waals heterostructure *Nature* **599** 582
[17] Fert A, Reyren N and Cros V 2017 Magnetic skyrmions: advances in physics and potential applications *Nat. Rev. Mater.* **2** 17031
[18] Röβler U K, Bogdanov A N and Pfleiderer C 2006 Spontaneous skyrmion ground states in magnetic metals *Nature* **442** 797–801
[19] Raju M, Yagil A, Soumyanarayanan A, Tan A K C, Almoalem A, Ma F, Auslaender O M and Panagopoulos C 2019 The evolution of skyrmions in Ir/Fe/Co/Pt multilayers and their topological Hall signature *Nat. Commun.* **10** 696
[20] Wu H *et al* 2020 Ferrimagnetic skyrmions in topological insulator/ferrimagnet heterostructures *Adv. Mater.* **32** 2003380
[21] Li P *et al* 2021 Topological Hall effect in a topological insulator interfaced with a magnetic insulator *Nano Lett.* **21** 84–90
[22] Ahmed A S *et al* 2019 Spin-Hall topological Hall effect in highly tunable Pt/ferrimagnetic-insulator bilayers *Nano Lett.* **19** 5683–8
[23] Dijkstra J, Weitering H H, Bruggen C F V, Haas C and Groot R A D 1989 Band-structure calculations, and magnetic and transport properties of ferromagnetic chromium tellurides (CrTe, Cr_3Te_4, Cr_2Te_3) *J. Phys.: Condens. Matter* **1** 9141
[24] Tang B *et al* 2022 Phase engineering of Cr_5Te_8 with colossal anomalous Hall effect *Nat. Electron.* **5** 224–32
[25] Meng L *et al* 2021 Anomalous thickness dependence of Curie temperature in air-stable two-dimensional ferromagnetic 1T-$CrTe_2$ grown by chemical vapor deposition *Nat. Commun.* **12** 809
[26] Fragkos S, Pappas P, Symeonidou E, Panayiotatos Y and Dimoulas A 2022 Magnetic skyrmion manipulation in $CrTe_2/WTe_2$ 2D van der Waals heterostructure *Appl. Phys. Lett.* **120** 182402
[27] Zhang X *et al* 2021 Giant Topological Hall Effect in van der Waals Heterostructures of $CrTe_2/Bi_2Te_3$ *ACS Nano* **15** 15710–9
[28] Chen J *et al* 2019 Evidence for Magnetic Skyrmions at the Interface of Ferromagnet/Topological-Insulator Heterostructures *Nano Lett.* **19** 6144–51
[29] Zhou L *et al* 2019 Topological Hall effect in bulk ferromagnet Cr_2Te_3 embedded with black-phosphorus-like bismuth nanosheets (arXiv:1903.06486)
[30] Li B, Zhang R, Zhou L, Wang L, Yan Z, He H and Wang G 2022 The construction of $Cr_2Te_3/Bi_2/Bi_2Te_3$ superlattice via reduction method by molecular beam epitaxy *Appl. Phys. Lett.* **120** 093102
[31] Takashiro T *et al* 2022 Soft-magnetic skyrmions induced by surface-state coupling in an intrinsic ferromagnetic topological insulator sandwich structure *Nano Lett.* **22** 881–7
[32] Xia H, Li Y, Cai M, Qin L, Zou N, Peng L, Duan W, Xu Y, Zhang W and Fu Y-S 2019 Dimensional crossover and topological phase transition in Dirac semimetal Na_3Bi films *ACS Nano* **13** 9647–54
[33] Zhang Z, Nie J, Zhang Z, Yuan Y, Fu Y-S and Zhang W 2022 Atomic visualization and switching of ferroelectric order in β-In_2Se_3 films at the single layer limit *Adv. Mater.* **34** 2106951
[34] Zhang T *et al* 2009 Experimental demonstration of topological surface states protected by time-reversal symmetry *Phys. Rev. Lett.* **103** 266803
[35] Lv H Y, Lu W J, Shao D F, Liu Y and Sun Y P 2015 Strain-controlled switch between ferromagnetism and antiferromagnetism in 1T-CrX_2 (X=Se, Te) monolayers *Phys. Rev.* B **92** 214419
[36] Freitas D C, Weht R, Sulpice A, Remenyi G, Strobel P, Gay F, Marcus J and Núñez-Regueiro M 2015 Ferromagnetism in layered metastable 1T-$CrTe_2$ *J. Phys.: Condens. Matter* **27** 176002
[37] Sun X *et al* 2020 Room temperature ferromagnetism in ultra-thin van der Waals crystals of 1T-$CrTe_2$ *Nano Res.* **13** 3358–63
[38] Zhang X *et al* 2021 Room-temperature intrinsic ferromagnetism in epitaxial $CrTe_2$ ultrathin films *Nat. Commun.* **12** 2492
[39] Xian J-J *et al* 2022 Spin mapping of intralayer antiferromagnetism and field-induced spin reorientation in monolayer $CrTe_2$ *Nat. Commun.* **13** 257
[40] Wang C, Zhou X, Zhou L, Pan Y, Lu Z-Y, Wan X, Wang X and Ji W 2020 Bethe-Slater-curve-like behavior and interlayer spin-exchange coupling mechanisms in two-dimensional magnetic bilayers *Phys. Rev.* B **102** 020402
[41] Park K, Heremans J J, Scarola V W and Minic D 2010 Robustness of topologically protected surface states in layering of Bi_2Te_3 thin films *Phys. Rev. Lett.* **105** 186801
[42] Li R, Nie J-H, Xian J-J, Zhou J-W, Lu Y, Miao M-P, Zhang W-H and Fu Y-S 2022 Planar heterojunction of ultrathin $CrTe_3$ and $CrTe_2$ van der Waals magnet *ACS Nano* **16** 4348–56
[43] Wang G *et al* 2011 Topological insulator thin films of Bi_2Te_3 with controlled electronic structure *Adv. Mater.* **23** 2929–32